JMEPEG (2013) 22:152–161
DOI: 10.1007/s11665-012-0219-y

1059-9495/$19.00

Design and Development of High-Velocity Slurry Erosion Test Rig Using CFD

H.S. Grewal, Anupam Agrawal, and H. Singh

(Submitted December 31, 2011; in revised form March 7, 2012; published online April 11, 2012)

Slurry erosion (SE) is commonly observed in almost all kinds of components and machineries involved in fluid (liquid) transfer and delivery. During design and development phase of these components, test rigs are usually required to evaluate their performance; however, only few detailed designs of test rigs are available for SE investigations. Among the existing designs of SE test rigs, most of them belong to rotary type. In the present study, design of a new type of SE test rig has been proposed, which is simpler in construction and working. This newly designed test rig could possibly eliminate some of the limitations (velocity-concentration interdependence and lack of acceleration distance) found in the existing set-ups. Calibration of the test rig was done for jet velocity and erodent concentration. Commissioning of the rig was undertaken by evaluating the effect of operating parameters (concentration and impingement angle) on the erosion rates of aluminum and cast iron. Results show that the rig was able to capture the traditional responses of ductile and brittle erosion behaviors being observed for these materials. Repeatability of the test rig was ensured, and the results were found to be within the acceptable error limits.

Keywords CFD, mechanical testing, slurry erosion, surface engineering

1. Introduction

Slurry erosion (SE) is a type of surface degradation process in which a stream of fluid entrained with abrasives impinges the surface with a velocity greater than 1 m/s (Ref 1). Erosion taking place at velocities greater than 6-9 m/s is termed as high-velocity erosion, and that occurring at lower velocities, as low-velocity erosion (Ref 1). The damage caused by erosion could be highly detrimental depending upon the severity of the conditions, which can even render the components from future service. These kinds of highly erosive conditions are mostly found in hydroturbines, propellers in marine applications, valves in the off-shore industry, petrochemical and utility plants, etc. (Ref 2–5). Owing to SE, machineries and components in these plants usually suffer huge economic losses, which could mount to millions of dollars. Quite a large number of studies could be found in the literature basically aiming at improving the erosive resistance properties of the existing materials, evaluating the alternatives, and understanding the basic mechanisms involved in the erosion process (Ref 6–8). Erosion is a very complex process, which involves number of interacting variables. Both the individual, as well as, the interactive properties of fluid and solid further add to complexity. As a result, even after 50 years since the first significant attempt made by Finnie (Ref 9), this process has not been completely understood, and attempts are being made to improve the know-how of the subject.

The various factors contributing toward the SE process can be categorized into three types (Ref 9, 10). The first category belongs to the factors corresponding to the operating conditions, such as velocity, impact angle, type of flow, fluid viscosity, and concentration of the erodents (Ref 9, 10). The second category corresponds to the factors related to the target materials, such as composition, microstructure, hardness, toughness, fatigue, yield and ultimate strengths, and work hardening, and additionally for the coatings, factors such as porosity, inter-splat bonding, and adhesion to substrate (Ref 9, 10). Under the third category, factors related to the erodents, such as composition, hardness, shape, size, and size distribution of the particles are considered (Ref 9, 10).

Erosion studies have been conducted in the literature using a number of different types of experimental set-ups, which include the rotary (pot- and Coriolis)-type test rigs (Ref 11, 12), jet-type test rigs (Ref 13), and whirling arm test rigs (Ref 14, 15). The most commonly used pot- and centrifugal-type test rigs suffer from an inherent defect of slurry aging. To avoid the slurry aging effect, replacement of the slurry is usually recommended. In addition to slurry degradation, rotary-type test rigs also lack the better control of test variables (impingement angle, velocity, and concentration) for which jet-type rigs are generally recommended (Ref 13). Jet-type test rig can be classified into re-circulating (RC) and non-recirculating (NRC) types. In the former type, abrasives are circulated again and again in the testing cycles for a pre-defined number of cycles, whereas in the latter case, the erodents are discarded after striking the target. The use of latter types of set-up eliminates the error induced due to fracturing and rounding of the erodent particles; on the other hand, former type is simple in construction and operation. Another issue related to NRC-type rigs is the complex interaction involved between concentration and velocity. Thus, a large number of erosion studies could be

H.S. Grewal, Anupam Agrawal, and **H. Singh**, School of Mechanical, Materials and Energy Engineering, Indian Institute of Technology Ropar, Nangal Road, Rupnagar, 140001 Punjab, India. Contact e-mails: harpreetsingh@iitrpr.ac.in.

found in the literature employing RC-type test rigs considering the complex nature of design of NRC-type erosion testers (Ref 7, 16–22). Moreover, in the test rigs where same slurry is re-circulated, such as in pot-, centrifugal-, or RC jet-type rigs, the control of erodent concentrations poses a problem due to regular evaporation of the water (fluid), the mechanical energy of the pumping system causes an increase in the temperature of the slurry, which results in the evaporation of the water from the slurry, the result of which would be a substantial variation in concentration. Therefore, an effective cooling system is required to eliminate this problem, which further needs better control and monitoring.

Some studies could be found in the literature (Ref 23, 24), where NRC-type rigs have been utilized to study the SE response of materials and coatings; however, a detailed design could not be found, limiting the possibility to reproduce them effectively. Moreover their complex design does not encourage researchers to adopt them. In this article, an attempt has been made to provide solutions to these problems, by suggesting a simple design of NRC-type test rig considering the interdependency of concentration and velocity.

1.1 Review of Jet-type Test Rigs

Jet-type rigs have been in most common use for SE experimentations. Table 1 lists some of the SE set-ups of the jet type being used by several investigators showing some of the important controllable parameters. In addition, Fig. 1 gives a schematic representation of different approaches of the used jet-type rigs, along with some observed limitations. A number of studies could be found in the open literature where a jet-type rig has been used for experimentation; however, only a few of them are of NRC type (Ref 23, 24). In this article, the design of NRC-type jet rig is discussed because of its capability to better simulate the actual erosive conditions, as discussed in previous section. Although NRC-type rigs have been employed by some authors for SE as seen in Table 1, a detailed description of these rigs so as to imitate them is scarce with an exception of that of Zu et al. (Ref 13), which also re-circulates the sand to some extent.

Among the various types of designs of jet-type erosion test rigs, the design suggested by Zu et al. (Ref 13) seems to be the most popular, since it has been employed by a large number of researchers (Ref 25–28). In this set-up, slurry is sucked at the entrance to the nozzle using an in-built ejector assembly from the container, wherein the erodent particles after striking the specimen fall back into the same container, causing the need of slurry replacement after some duration. The test rig was capable of attaining a velocity of 8 m/s at 30% concentration. However, the limited velocity range and the inadequate distance for the erodents to accelerate to the velocity of the fluid limits the scope for its adoption. As pointed out by Finnie (Ref 9) and Wood and Wheeler (Ref 29), there is a need for an acceleration tube so that entrained particles could approach the stream velocity. Inadequate travel distance available for the erodent particles to accelerate to the velocity of the fluid stream could devoid the assumption that erodent particles travel at the velocity of fluid. Computational fluid dynamics (CFD) could successfully be used to estimate and optimize the length of an acceleration tube. Another design alternative for jet-type SE test rig was proposed by Matsumura (Ref 30), namely, jet-in-silt, wherein specimens submerged inside the fluidized bed were subjected to a jet of clean water coming from the nozzle placed beneath the sample. The particles of the sand present in the slurry were assumed to strike the specimen at the same velocity as that of the jet, with a concentration equivalent to that of the slurry mixture. A whirling arm-type tester has been suggested by Lin and Shao (Ref 15), where specimens rotating on an arm are impinged by dropping slurry in vacuum to avoid error due to aerodynamics effect of the particles. A more recent design has been suggested by Iwai et al. (Ref 31), named as micro-jet SE tester for erosion performance ranking of the coatings. In this tester, alumina particles of size 1 μm were used as erodents and impinged on the samples at a velocity of 100 m/s (authors were not able to accurately measure the velocity). However, as mentioned by the authors, a very low level of mass loss caused difficulty in the erosion assessment, requiring use of advanced characterization techniques such as atomic force microscopy (AFM) for topographical and erosion characterization.

Out of the various types of the SE rigs available, the jet-type rigs seem to provide better control over various parameters, such as velocity, impact angle, and concentration, in comparison with rotary-type test rigs. In addition to these advantages, jet-type rigs can be designed using a NRC scheme learnt from the literature, thus reducing experimental errors. Moreover, the flow conditions found in the jet-type rigs are more close to those found in actual conditions (turbines, valves, etc.).

Several investigations indicate that the velocity affects the erosion significantly (Ref 32, 33). The level of velocities found

Table 1 Review of jet-type SE test rigs, found in the literature

Type	Max. velocity, m/s	Concentration, wt.%	Sample size, mm × mm	Nozzle diameter, mm	Sand suction method	References
Semi recirculating	8	30	30 × 35	4.5-6.5	Vacuum suction at nozzle	13
Non-recirculating	117.3(a)	0.0028-0.0017	20 × 20	4	Vacuum at nozzle	23
Recirculating	30	2.1	40 × 40	6-10	NA	7
Recirculating	15.2	25	…	1.8	NA	30
Recirculating	17	20	25 × 26	4.76	NA	19
Recirculating	30	30	…	2	…	20
Recirculating	17	0.05	…	4	NA	21
Non-recirculating	75	0.4	45 × 17	5	Vacuum suction at nozzle	24
Recirculating	27	0.75	40 × 40 or 22 × 68	Variable	NA	22

(a) Probably the highest velocity used in SE testing rigs ever, but too low a concentration value could limit the direct application of its results to actual conditions persisting in fluid machineries, especially hydro-turbines. Detailed design not available

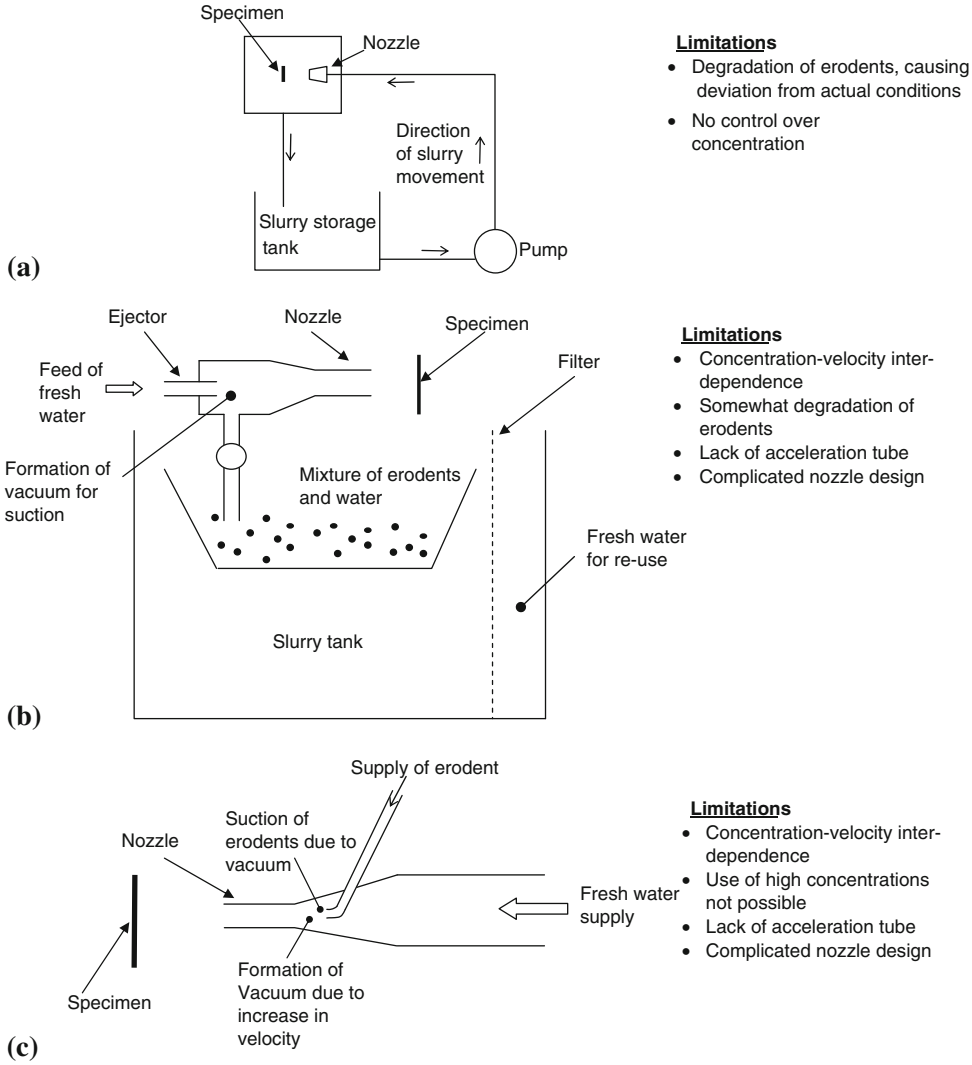

Fig. 1 Schematic representation of different types of test rigs employed in the literature for SE studies: (a) Generally used RC jet-type test rig, (b) NRC jet-type set-up proposed by Zu et al. (Ref 13), and (c) NRC jet-type set-up employed by Lin et al. (Ref 23) and Santa et al. (Ref 24)

in the actual conditions could be somewhere in the range of 1-30 m/s, whereas in some extreme cases, higher values could also be found. In most of the actual working conditions, the erodent particles strike the target surfaces, thereby causing the erosion of the surfaces. Simultaneously, fracturing, disintegration, and rounding-off of the erodent particles could also take place (Ref 34). This necessitates conducting the testing using NRC-type rigs. A high-velocity air jet erosion tester has also been designed by Wood and Wheeler (Ref 29); however, a similar design does not seem viable for this study owing to differences in operating conditions.

Designing of the set-up was undertaken with the help of a CFD approach. CFD is a powerful simulation tool which could aid in design process of such a rig. Using the CFD, various components of rig could be easily and economically designed. Without the availability of such a tool, designing could be very tedious, lengthy, and time consuming, involving numerous on-field trials and thus causing wastage of useful resources. Simulated results offered by CFD could possibly save huge amount of physical efforts involved during the development of such rigs. Real-time interactions offered by CFD could be advantageous as they show as to how changes in a particular design parameter affect the output without actual testing. The proposed NRC-type high-velocity SE test rig is capable of attaining velocities, as high as, 25 m/s. Such rigs could help in determining the erosion ranking of materials under conditions similar to actual environments.

The sensitivity of NRC rigs to the operating conditions is mainly due to the sand introduction methods employed. The mixing of sand in water is performed through suction pressure created either at the nozzle or by venturi placed in a water line. Therefore, the amount of sand sucked would depend upon the velocity of water making concentration dependent upon the velocity of the flowing water. Both these methods also have their drawbacks owing to inadequate distance for particle acceleration when sucked at nozzle in the former case; and loss of pressure with the use of venturi in the flow line in the latter case. In the current design of this study, both these problems are taken care of by proposing an alternative method of erodent mixing. Moreover, an attempt has been made to keep the design simpler. The proposed design would also eliminate the inter-dependence of the erodent concentration and the velocity of liquid.

2. Design of Test Rig

2.1 Design Specifications

Keeping in view of the actual working conditions found in hydraulic machineries, such as pumps, hydroturbines, and other in-line components, various specifications for the SE tester were decided, which are given in Table 2. These specifications have been used as limiting parameters in the design process. In fluid machineries, erodent (sand) particles usually impinge at various angles ranging from near zero to 90°. Slurry concentration values are often limited to avoid excessive damage to turbine components to a maximum range of 4000-5000 ppm (0.4-0.5 wt.% assuming sand particles in water) (Ref 35). In this study, a test rig capable of producing maximum concentration of 1 wt.% has been designed, so as to conduct the testing under aggressive conditions. Most of the hydro power projects and pumps are installed with a desilting plants and filters, to remove the excessively larger sized sand particles. Quite often particles below 0.3 mm size pass through the components and cause damage. Therefore, this test rig has been designed to carry sand particles from 0.025 to 0.45 mm in size entrained in water.

Table 2 Proposed specifications of test rig

Parameter	Value
Impact velocity	25 m/s
Erodent's concentration	1 wt.% max (10,000 ppm)
Impingement angle	10-90°
Stand off distance	150 mm max
Erodent size	25-500 μm
Erodent type	No constraint
Erodent shape	No constraint
Test material	Bulk or coating metals, alloys, ceramics and polymers

2.2 Layout

The type of test rig proposed in this article may be regarded as a hybrid of NRC- and RC-type rigs. In the present design, the problems such as the lack of acceleration distance for the particles and pressure drop in line because of the venturi are taken care of by the suction and mixing of the sand through an auxiliary pump. The auxiliary pump, as shown in Fig. 2, is made to suck the sand from the hopper (not shown) at its suction side along with the water. The mixture of sand and water is pumped and is injected into the main line (long acceleration tube) connected with the output of the main pump. The mixture is then made to flow through the tungsten carbide nozzle, which converts the pressure energy into kinetic energy. The sample fixed in the specimen holder can be moved to various locations so as to achieve variations in the impingement angle and stand-off-distance. With the help of this scheme, the mixing of the sand in the water can be done easily without causing the pressure drop in the main line as shown in Fig. 3. Also the problem due to limited acceleration distance has been taken care of utilizing a long acceleration tube. After impingement, the slurry is collected inside the slurry tank, as shown in Fig. 2, from where it is filtered, and clean water is pumped back into the main tank. To control the flow rates, a bypass valve is connected with the main pump with the help of which, the quantity of water flowing into the mainline can be easily varied and thereby the impingement velocity. The amount of sand sucked could be controlled with the help of control valves, fitted inside the mixing chamber. For frequent monitoring, a flow meter and pressure and vacuum gauges are installed on the suction and delivery sides of the pumps and nozzle.

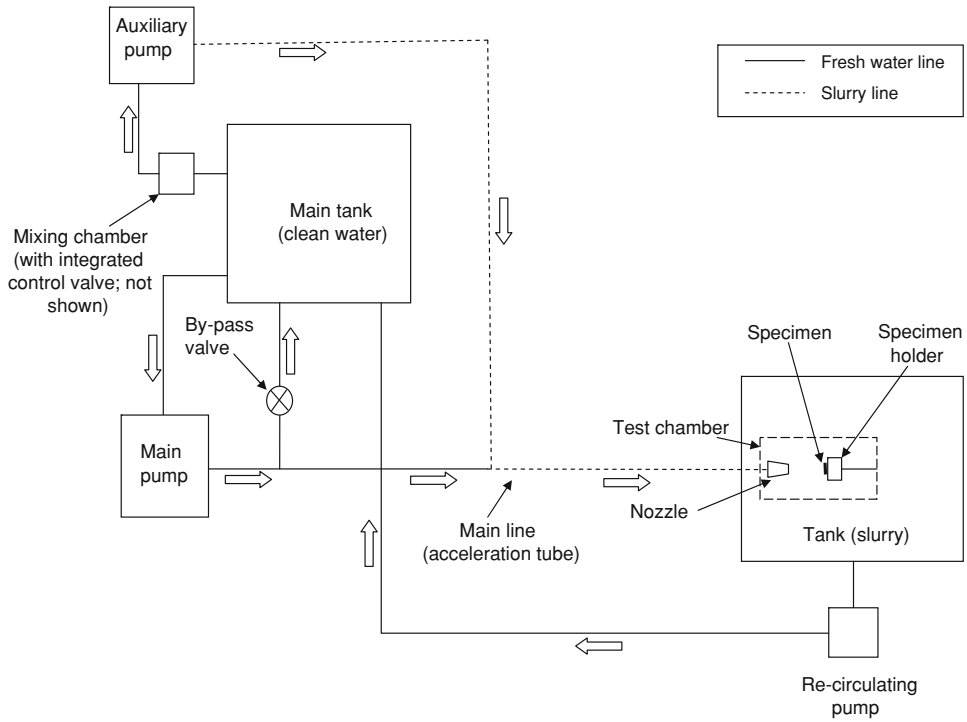

Fig. 2 Layout of the proposed experimental set-up

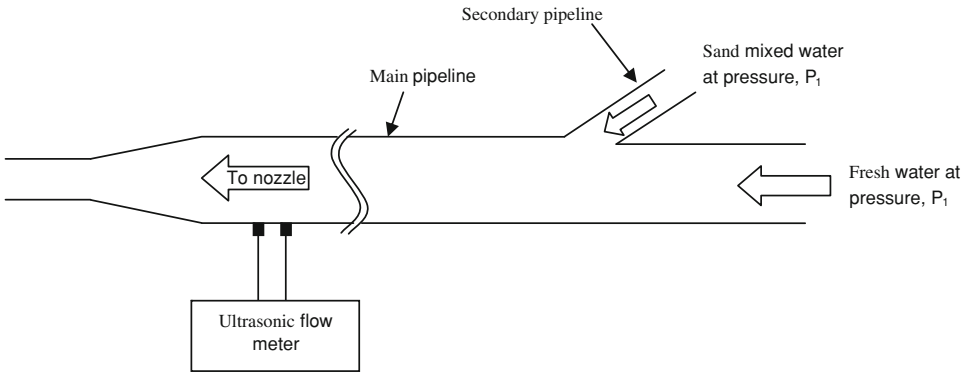

Fig. 3 Scheme of mixing slurry with fresh water

Calibrations of all the experimental parameters have been conducted and are presented in subsequent sections.

2.3 Modeling Procedure

For CFD simulations, commercially available package FLUENT 6.3 was employed. To construct and mesh the geometry, GAMBIT 2.4.6 was utilized with quadrilateral elements to discretize the geometry. To start with, elements of uniform size of 0.5 mm were used. Further, the size of the mesh was optimized using adaptive meshing resulting in a finer mesh at a location of mixing of particles with main stream fluid and inside the nozzle. Steady-state CFD simulations were conducted using standard κ-ε turbulence model with 5% intensity. Before the injection of the particles, a convergence criterion of 10^{-5} for continuity of the flow field was employed. After convergence, particles were injected through secondary pipeline as shown in Fig. 2, distributed uniformly over whole of the particle injection surface. For validation, outlet velocities of fluid from nozzle, as obtained from CFD simulation, were compared with those obtained experimentally at different sets of velocities, and they were found to be in close approximation within an error band of 3%."

2.4 Selection of Components

Various important components required for the test rig include nozzle, pumps along with some necessary connecting members, filtering system, flow and pressure measuring instruments, and storage tanks. The size of the nozzle, after going through the relevant literature (Table 1) and a brainstorming session, was selected and fixed to be 4 mm. A larger nozzle would require an increase in the pumping capacity, thus enhancing the overall set-up cost. A 4-mm size was selected, as it is the minimum size used in the literature; moreover, it is also believed that further reduction in the nozzle size would cause an increase in the interaction effect among the erodent particles. The remaining parameters of the nozzle were optimized utilizing standard κ-ε turbulent flow CFD model. The final detailed design of the nozzle is presented in Fig. 4, and its CFD results are shown in Fig. 5. A straight portion at the exit of the nozzle would ensure in containing the diverging effect of the jet.

Selection of pump for the required jet velocity is an important issue of concern while designing such type of experimental rigs. In order to attain a velocity of the order of 25 m/s from the nozzle, using Bernoulli's equation, a flow rate of 3.2×10^{-4} m^3/s was determined at a minimum of 3 bar

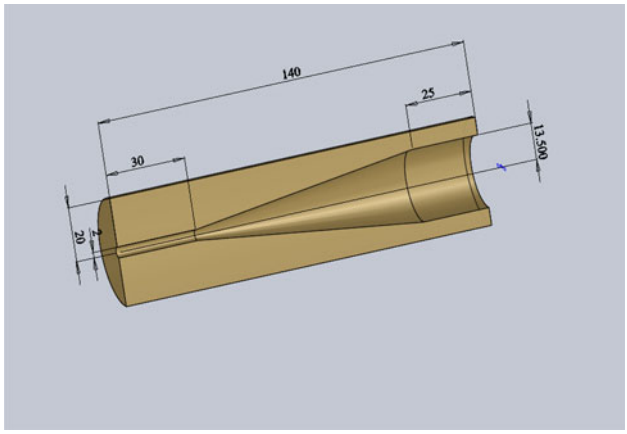

Fig. 4 Details of nozzle employed in the set-up

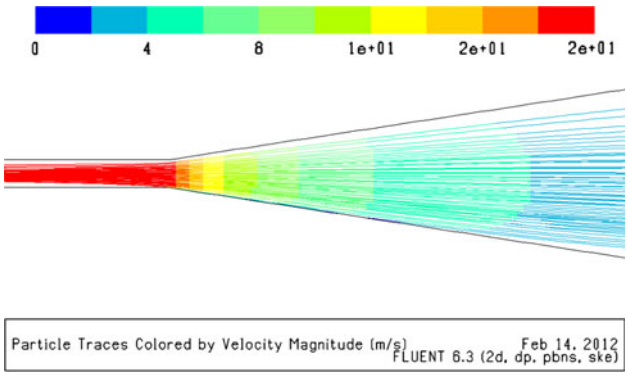

Fig. 5 CFD analysis of nozzle

pressure. Thus, two pumps capable of providing a pressure of 3 bar at the required discharge were selected, one of which used as an auxiliary pump was of slurry pump type as could be seen in the layout shown in Fig. 2. A slurry pump was used as an auxiliary pump to eliminate the problem of leakage in the circuit.

Length of the acceleration tube was calculated using CFD. Optimization of the tube length and injection angle was done with the help of CFD to ensure complete mixing of the sand with water. Injection angle is an important parameter which needs to be selected judiciously. A very high angle would cause the particles to strike the pipe wall; thus, the injection angle was

preferred to be kept as small as possible. To avoid this problem, analyses were conducted at various angles ranging from 10° to 30°. As seen from Fig. 6, those particles injected at 10° injection angle are well carried away by the water coming from the main pump, as compared to those injected at 30°. Although some of the particles still strike the pipe when injection takes place at 10°, further reduction is not feasible due to physical constraints. To get an optimized tube length, various iterations were conducted by varying the tube length starting from 0.5 m, for particle size distribution (PSD) of 50-500 μm as found in hydroturbines, pumps, and other fluid transport equipments. The effect of tube length upon the velocity of the particles could be analyzed from Fig. 7. The velocities of the particles shown in Fig. 7 are the averages of 60 particle streams at any particular cross-section. It is seen that tube of length 1 m would be sufficient for particles to approach the stream velocity. Further details of this fact could be found in Fig. 8(a), where particle tracks are plotted for 1-m tube length. Difference between particle velocity (V_p) and stream velocity (V_l) versus the length of the tube is plotted in Fig. 8(b). From Fig. 8, it is seen that particles are approaching the streamline velocity. In Fig. 8(b), a sharp transition in ($V_p - V_l$) could be observed. It is worthwhile to mention here that the position of the first point (point 1 in Fig. 8b) of transition corresponds to the entry level of the nozzle, where the stream velocity increases abruptly making the particles to lag behind. The position of second sharp transition correspond to the entry level of straight portion of nozzle of ∅ 4 mm, at which the particles seem to accelerate up and approach the stream velocity. The benefit of using a straight portion inside the nozzle could easily be confirmed from these results. Effect of stream velocity was also studied, and it was found that even for low main stream velocities of around 0.2 m/

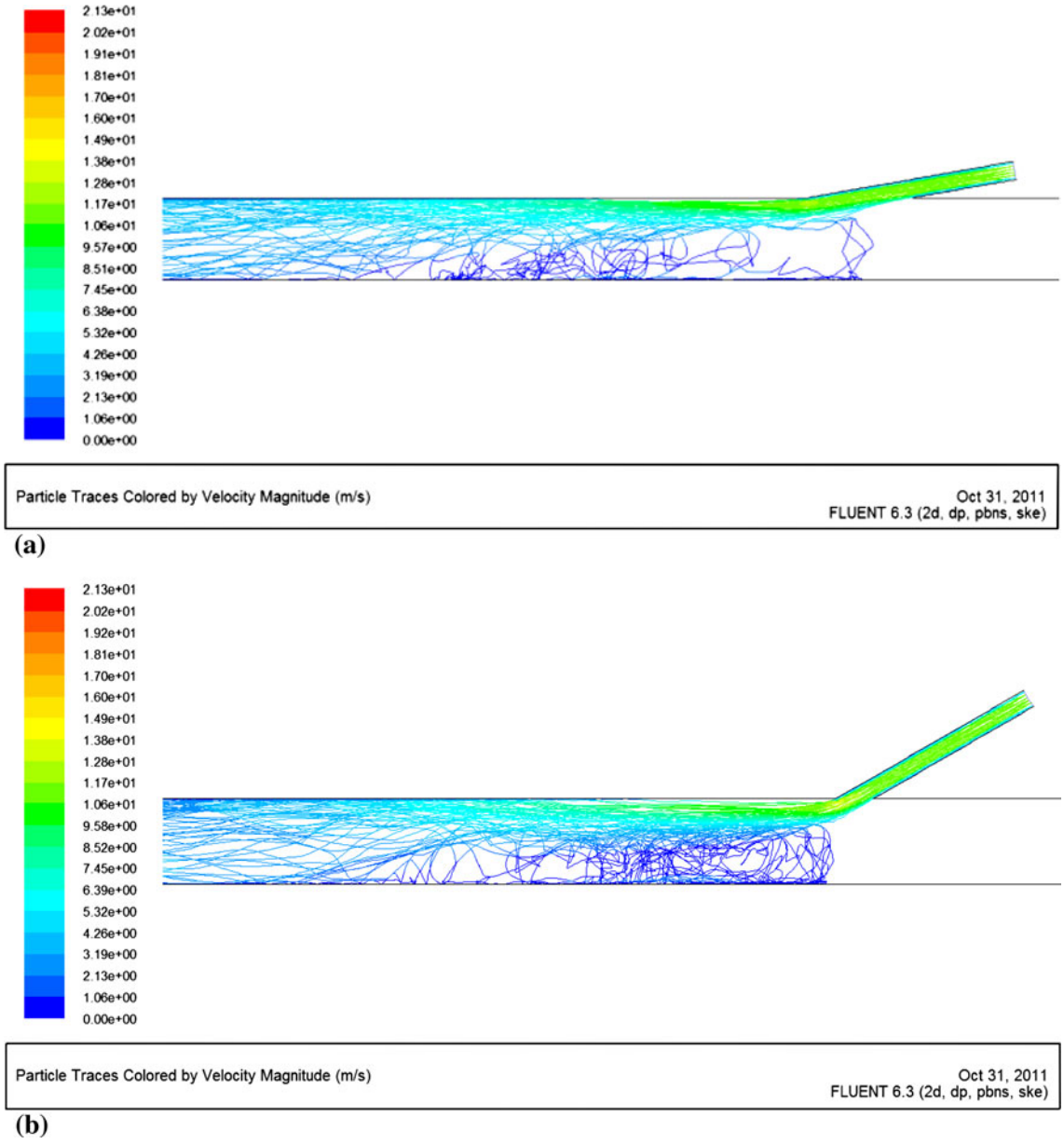

Fig. 6 Effect of injection angle on the particles trajectories (a) injection angle 10° and (b) injection angle 30°

s, the particles are well carried away. This indicates that mixing and transportation of particles is not affected significantly by main stream velocity.

3. Instrumentation

Regular monitoring of the testing parameters is essential to conduct experimentation in a well-controlled manner. Advanced instruments such as particle image velocimetry (PIV) and high speed photography have been successfully used for the measurement of velocity and concentration in a jet of slurry; however, their higher initial costs place restrictions on them to be commonly used. Thus, some low-cost instruments for the measurement of flow parameters are used to demonstrate cost-effective testing methods.

For real-time monitoring of flow velocity, an ultrasonic flow meter (UFM) [Shenitech, USA, model: ST301] capable of measuring velocities up to 16 m/s of flow in a 25-mm pipe was used. UFM measures the flow rate and the velocity of the liquid flowing through the pipe. Being a non-contact-type, ultrasonic-based flow meter does not provide any disturbance to the flow as is the case with electromagnetic-type flow meter.

Measurement of the exact concentration at the nozzle exit is a very important and difficult task. Concentration was measured by filling the hopper with a known amount of sand, and calculating the amount of sand that has been sucked and quantity of water that flows through the nozzle in a given time. After knowing these quantities, the concentration in terms of commonly used units (g/min or g/L or ppm) could be easily calculated. Concentration of the slurry coming out of the nozzle was also evaluated using the evaporation method as suggested by ASTM standard D-3977.

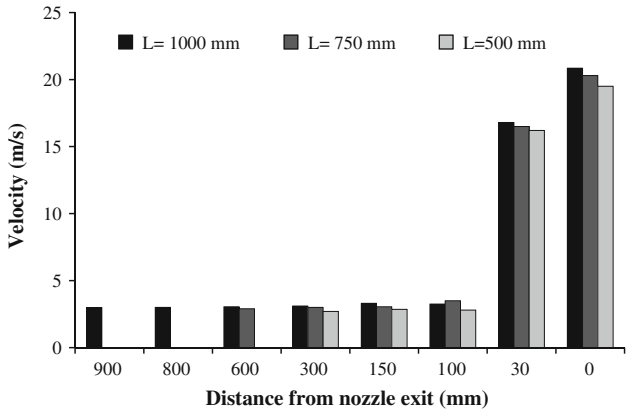

Fig. 7 Effect of acceleration tube length on particle velocity at different cross sections (velocity reported is the average of 60 particle streams)

4. Calibration

Calibration is essential for any equipment in order to produce some reliable data with good repeatability. For the existing test rig, calibration of impingement velocity and concentration was undertaken. The variation in the particle size after it passes through the auxiliary pump was also studied.

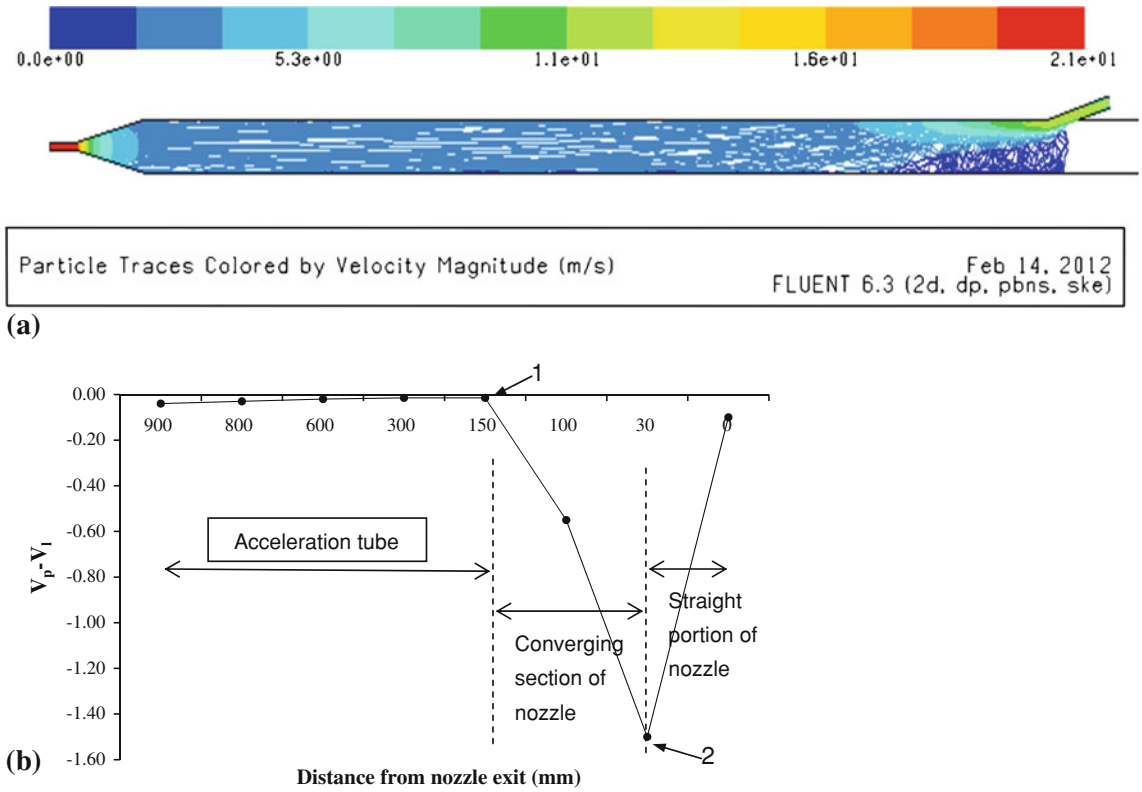

Fig. 8 (a) Particle trajectories in 1-m-long acceleration tube with injection angle 10°. (b) Variation of difference between particle (V_p) and stream (V_l) velocities along the length of the acceleration tube

Table 3 Calibration of slurry concentration

Amount of sand used, g	Time taken, min	Concentration, wt.% (ppm)	Concentration calculated as per ASTM standard procedure, wt.% (ppm)
155	10	0.1 (1000)	0.101 (1010)
387.5	10	0.25 (2500)	0.257 (2570)
775	10	0.5 (5000)	0.505 (5050)
1162.5	10	0.75 (7500)	0.76 (7600)

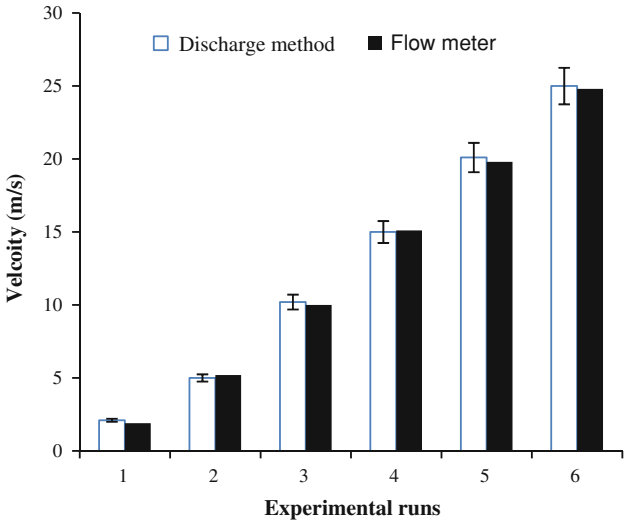

Fig. 9 Calibration results of velocity

4.1 Calibration of Concentration

As discussed in the preceding section, desired concentration of the erodent particles in a jet of slurry could be achieved by making a known quantity of sand to flow in a measured quantity of water in a predetermined time. By varying the quantity of sand sucked in a unit time, the variation in the concentration could be achieved. For each calibration test, a known weight of sand as shown in Table 3 was made to flow through a 1.5-mm orifice with water velocity of 20 m/s. Table 3 shows the values of the concentrations calculated with both the methods, and it could be seen that the maximum error between evaporation and sand flow rate method was around 2%. These results show that premixed quantity method could be utilized for attaining a desired concentration with a maximum error of 2%, compared with the standard method.

4.2 Calibration of Velocity

Fluid quantity was measured using non-obstruction-type UFM fitted at the outer surface of the pipe. UFM was re-calibrated on-site with a water collection method (collecting and weighing the water coming out of the nozzle). Figure 9 shows the readings of the UFM compared with the discharge obtained by water collection method. Reproducibility of the results was established by repeating the process three times for each discharge rate. The results show nearly the same results from both the methods with a maximum error of around 0.5%, which show the accuracy and reproducibility of the UFM. Velocity of the jet could be calculated using continuity equation.

5. Rig Commissioning

Commissioning and calibration of the test rig is an important task, before recommending the erosion test rig for further experimentation. For this purpose, polished samples of aluminum (Al) and cast iron (CI) of size $20 \times 20 \times 5$ mm^3 were prepared, which have been chosen, respectively, as the representative cases of ductile and brittle materials. The selection of test materials was made so as to investigate whether the rig was capable of clearly distinguishing the ductile and brittle modes of erosion mechanisms as observed in these test materials. One way of identifying whether materials would show a ductile or brittle mode of erosion is by observing their erosion response with respect to impact angle. Ductile materials show maximum erosion at lower impact angles (20-30°), whereas brittle materials at around normal impact angles (Ref 8, 36–38). To evaluate this ductile-brittle erosion behaviors, both cast iron and aluminum samples were tested at two impact angles (20° and 90°) at a velocity of 25 m/s. To evaluate the response shown at different concentrations, the samples were tested at 0.25 wt.% (2500 ppm) and 0.5 wt.% (5000 ppm) erodent load, using foundry sand as the erodent. The morphology of the particles could be analyzed from Fig. 10(a), which represents a mixture of mostly irregular-shaped particles along with the presence of some round-shaped particles. Sand used for testing was alienated using sieves of standard sizes (450, 300, 220, 150, and 100 μm) with the help of sieve shaker. The quantity of sand collected in each sieve was measured for calculating PSD of the sand. The weight of the sand collected in each sieve divided by the total weight of the sand used would provide the weight distribution of each respective size. The particle sizes of the erodent sand were kept within the range of 425-100 μm, and the size distribution is shown in Fig. 11. Testing was conducted with 1 and 2 kg of sand at 0.25 and 0.5 wt.% concentrations, respectively. Weight measurements of the eroded samples were taken after washing with acetone and drying in air on precision weighing balance of 0.01 mg accuracy. The weight loss of the samples was converted into equivalent amount of volume loss, using the density values of 2700 kg/m^3 for Al and 7800 kg/m^3 for CI.

6. Discussion

The variation in the volume loss of the Al and CI at different impact angles and concentrations is shown in Fig. 12(a) and (b) with respect to erodent mass. The variation in the erosion rates with respect to impact angle suggests that Al is showing ductile erosion behavior (maximum erosion at 20°), whereas CI is showing, as expected, a brittle erosion behavior (maximum

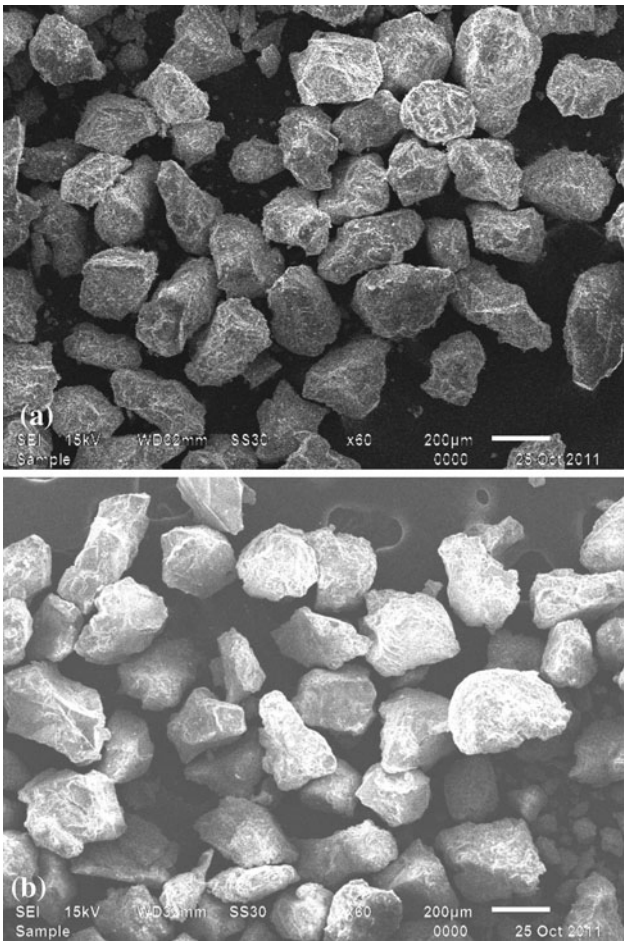

Fig. 10 SEM micrographs of sand particles: (a) unused and (b) sand pumped

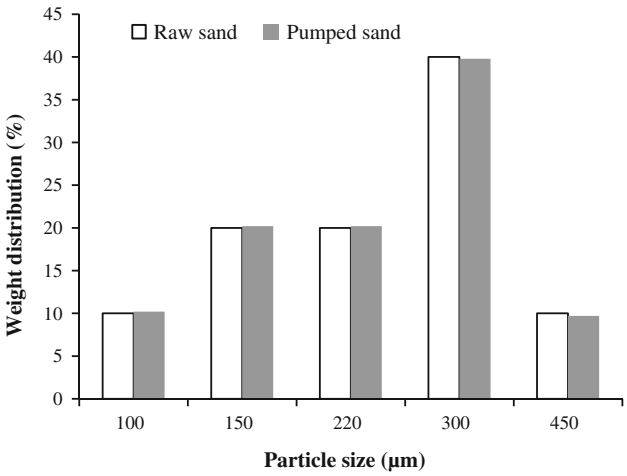

Fig. 11 PSD of used sand

erosion at 90°). Hence, the behaviors of both the target materials are in accordance with those found in the published study (Ref 8, 37, 38). Comparison of the Fig. 12(a) and (b) shows almost twice the erosion results at 0.5 wt.% concentration as compared to that tested at 0.25 wt.%. This increase in

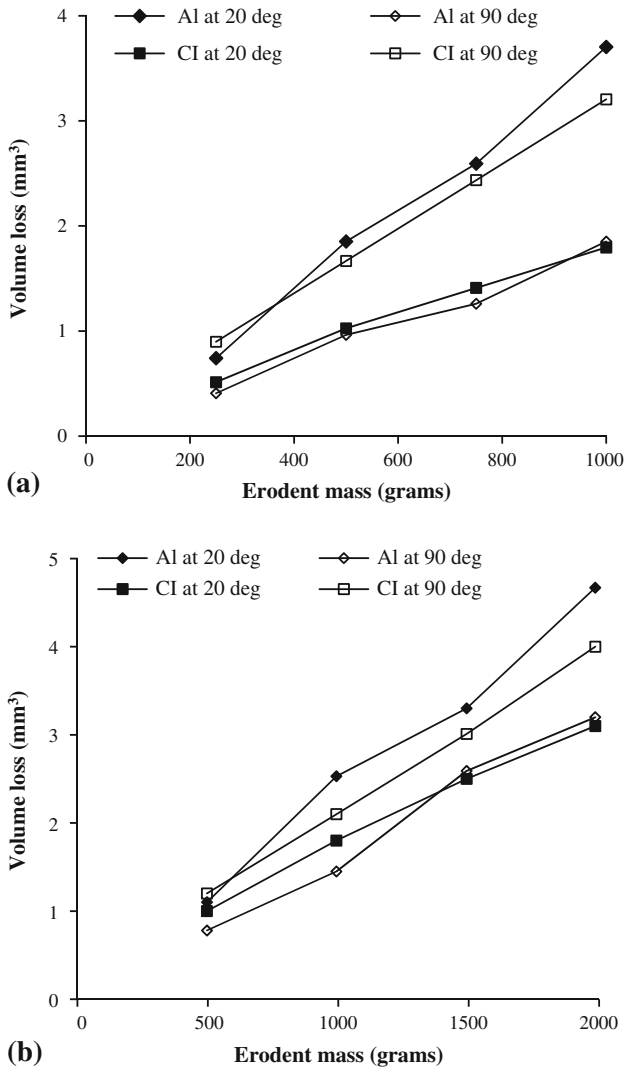

Fig. 12 Variation of erosion rate of Al and CI at 20° and 90° impact angles with respect to erodent mass, at two different concentrations: (a) concentration 0.25 wt.% (2500 ppm), and (b) concentration 0.5 wt.% (5000 ppm)

the erosion rate is due to a two-fold increase in the number of particles striking the specimen at a particular time (Ref 12, 39).

Variation in the volume loss with respect to erodent mass could also be accessed from Fig. 12(a) and (b). The slopes of the volume loss curves for both Al and CI suggest a linear variation of the volume loss with respect to erodent mass. A higher erosion rate for Al as compared with CI at lower impingement angles is in response to the higher hardness of the CI as compared with Al. At lower impingement angles, micro-cutting mechanism of erosion is observed (Ref 8, 9); thus, with the increase in hardness, material shows more resistance to cutting mechanism.

The sand sampled after passing through the SE pump showed no observable size variation as shown in Fig. 10 and 11; thus, it could be concluded that properties of the erodent did not degrade after passing through the pump. These results help in strengthening our belief that the size of the erodent which strikes the specimen is the same as that of the latter which has been fed into the system, and no significant degradation of the erodent took place.

7. Conclusion

Design and development of a new jet-type SE test rig has been presented in the article. The main focus while designing the rig was concentrated toward simplicity in construction, while reducing, if not eliminating, the flaws in the existing jet-type SE rigs. Although designs of many types of solid particle erosion test rigs and rotary-type SE test rigs could be found in the literature, only a few such detailed designs were available for SE rigs. In the proposed design, although the maximum velocity attainable was limited to 25 m/s, the same can easily be increased depending upon the pumping capacity. The jet velocity and sand concentration were found to be independent of each other, providing the feasibility for further improvement in the jet velocities without worrying about concentration. The test rig was calibrated for velocity and for the sand concentration ranging from 0.1 wt.% (1000 ppm) to 1 wt.% (10,000 ppm). Commissioning of the rig was conducted using aluminum and cast iron samples tested at different levels of concentration and impingement angles. The results were consistent with those found in the literature with aluminum showing maximum erosion at around 20° impingement angle, whereas cast iron did at normal impingement. Testing conducted at 0.5 wt.% concentration showed almost twice the erosion as compared to the erosion at 0.25 wt.% concentration. The experience with the test rig established its simplicity at the operational and designing levels with testing procedure being almost automated.

Acknowledgments

The authors are grateful to Mr. Ram Kumar, Junior Lab attendant, IIT Ropar for his help during fabrication of this test rig.

References

1. *ASM Handbook, Volume 18, Friction, Lubrication and Wear Technology*, ASM International, Materials Park, 1992
2. B.S. Mann and V. Arya, Abrasive and Erosive Wear Characteristics of Plasma Nitriding and HVOF Coatings: Their Application in Hydro Turbines, *Wear*, 2001, **249**(5–6), p 354–360
3. R.J.K. Wood, Erosion-Corrosion Interactions and Their Effect on Marine and Offshore Materials, *Wear*, 2006, **261**(9), p 1012–1023
4. R.J. Llewellyn, S.K. Yick, and K.F. Dolman, Scouring Erosion Resistance of Metallic Materials Used in Slurry Pump Service, *Wear*, 2004, **256**(6), p 592–599
5. M. Miyasaka, K.I. Sugiyama, M. Noguchi, and H. Yakuwa, Erosion-Corrosion of Fluid Machinery and Environmental Equipment, *Zairyo to Kankyo/Corros. Eng.*, 2008, **57**(3), p 111–117
6. T. Manisekaran, M. Kamaraj, S.M. Sharrif, and S.V. Joshi, Slurry Erosion Studies on Surface Modified 13Cr-4Ni Steels: Effect of Angle of Impingement and Particle Size, *J. Mater. Eng. Perform.*, 2007, **16**(5), p 567–572
7. R.J.K. Wood, B.G. Mellor, and M.L. Binfield, Sand Erosion Performance of Detonation Gun Applied Tungsten Carbide/Cobalt-Chromium Coatings, *Wear*, 1997, **211**(1), p 70–83
8. I. Finnie, Some Reflections on the Past and Future of Erosion, *Wear*, 1995, **186–187**(Part 1), p 1–10
9. I. Finnie, Erosion of Surfaces by Solid Particles, *Wear*, 1960, **3**(2), p 87–103
10. H.C. Meng and K.C. Ludema, Wear Models and Predictive Equations: Their Form and Content, *Wear*, 1995, **181–183**(Part 2), p 443–457
11. W. Tsai, J.A.C. Humphrey, and I. Cornet, Experimental Measurement of Accelerated Erosion in a Slurry Pot Tester, *Wear*, 1981, **68**, p 289–303
12. H.M. Clark, H.M. Hawthorne, and Y. Xie, Wear Rates and Specific Energies of Some Ceramic, Cermet and Metallic Coatings Determined in the Coriolis Erosion Tester, *Wear*, 1999, **233–235**, p 319–327
13. J.B. Zu, I.M. Hutchings, and G.T. Burstein, Design of a Slurry Erosion Test Rig, *Wear*, 1990, **140**, p 331–344
14. A. Abouel-Kasem, Y.M. Abd-elrhman, K.M. Emara, and S.M. Ahmed, Design and Performance of Slurry Erosion Tester, *J. Tribol.*, 2010, **132**(2), p 021601–021610
15. F.Y. Lin and H.S. Shao, Effect of Impact Velocity on Slurry Erosion and a New Design of a Slurry Erosion Tester, *Wear*, 1991, **143**(2), p 231–240
16. R.C. Shivamurthy, M. Kamaraj, R. Nagarajan, S.M. Shariff, and G. Padmanabham, Influence of Microstructure on Slurry Erosive Wear Characteristics of Laser Surface Alloyed 13Cr-4Ni Steel, *Wear*, 2009, **267**(1–4), p 204–212
17. S. Shrestha, T. Hodgkiess, and A. Neville, Erosion-Corrosion Behaviour of High-Velocity Oxy-Fuel Ni-Cr-Mo-Si-B Coatings Under High-Velocity Seawater Jet Impingement, *Wear*, 2005, **259**(1–6), p 208–218
18. K. Sugiyama, S. Nakahama, S. Hattori, and K. Nakano, Slurry Wear and Cavitation Erosion of Thermal-Sprayed Cermets, *Wear*, 2005, **258**(5–6), p 768–775
19. S. Turenne, The Effect of Sand Concentration on the Erosion of Materials by a Slurry Jet, *Wear*, 1989, **133**, p 95–106
20. N. Yngve, Material Removal Mechanism of Ni(200) When Eroded by a Slurry at 30° Incidence, *Wear*, 1985, **105**(2), p 123–130
21. A. Neville and B.A.B. Mcdougall, Erosion- and Cavitation-Corrosion of Titanium and Its Alloys, *Wear*, 2001, **250**, p 726–735
22. J. Suchánek, V. Kuklík, and E. Zdravecká, Influence of Microstructure on Erosion Resistance of Steels, *Wear*, 2009, **267**(11), p 2092–2099
23. M. Lin, L. Chang, H. Lin, C. Yang, and K. Lin, A Study of High-Speed Slurry Erosion of NiCrBSi Thermal-Sprayed Coating, *Surf. Coat. Technol.*, 2006, **201**(6), p 3193–3198
24. J.F. Santa, L.A. Espitia, J.A. Blanco, S.A. Romo, and A. Toro, Slurry and Cavitation Erosion Resistance of Thermal Spray Coatings, *Wear*, 2009, **267**(1–4), p 160–167
25. Y. Li, G.T. Burstein, and I.M. Hutchings, Influence of Environmental Composition and Electrochemical Potential on the Slurry Erosion-Corrosion of Aluminium, *Wear*, 1995, **181–183**(Part 1), p 70–79
26. G.T. Burstein and K. Sasaki, Effect of Impact Angle on the Slurry Erosion-Corrosion of 304L Stainless Steel, *Wear*, 2000, **240**(1–2), p 80–94
27. Q. Fang, P. Sidky, and M.G. Hocking, Erosive Wear Behaviour of Aluminium Based Composites, *Mater. Des.*, 1997, **18**(4–6), p 389–393
28. G.C. Saha, T.I. Khan, and G.A. Zhang, Erosion-Corrosion Resistance of Microcrystalline and Near-Nanocrystalline WC-17Co High Velocity Oxy-Fuel Thermal Spray Coatings, *Corros. Sci.*, 2011, **53**(6), p 2106–2114
29. R.J.K. Wood and D.W. Wheeler, Design and Performance of a High Velocity Air-Sand Jet Impingement Erosion Facility, *Wear*, 1998, **220**(2), p 95–112
30. M. Matsumura, *Wear of Materials 1983: Presented at the International Conference on Wear of Materials*, K.C. Ludema, Ed., April 11–14, 1983 (Reston, VA), American Society of Mechanical Engineers, 1983
31. Y. Iwai, T. Honda, H. Yamada, T. Matsubara, M. Larsson, and S. Hogmark, Evaluation of Wear Resistance of Thin Hard Coatings by a New Solid Particle Impact Test, *Wear*, 2001, **251**(1–12), p 861–867
32. B.A. Lindsley and A.R. Marder, The Effect of Velocity on the Solid Particle Erosion Rate of Alloys, *Wear*, 1999, **225–229**(Part 1), p 510–516
33. A.V. Levy, The Erosion-Corrosion Behavior of Protective Coatings, *Surf. Coat. Technol.*, 1988, **36**, p 387–406
34. S. Lathabai and D.C. Pender, Microstructural Influence in Slurry Erosion of Ceramics, *Wear*, 1995, **189**(1–2), p 122–135
35. T.P. Singh, J. Chandrashekhar, and A.K. Agrawal, Analysis of Water and Sediment Flow in Desilting Basin of a Run-of-River Hydroelectric Project, *International Conference on Small Hydropower*, Oct. 22–24, 2007 (Srilanka)
36. H.M. Clark, A Comparison of Particle Impact in Gas-Solid and Liquid-Solid Erosion, *Wear*, 1995, **186–187**(Part 2), p 465–472
37. B.D. Jana and M.M. Stack, Modelling Impact Angle Effects on Erosion-Corrosion of Pure Metals: Construction of Materials Performance Maps, *Wear*, 2005, **259**, p 243–255
38. Y.I. Oka, S. Mihara, and T. Yoshida, Impact-Angle Dependence and Estimation of Erosion Damage to Ceramic Materials Caused by Solid Particle Impact, *Wear*, 2009, **267**(1–4), p 129–135
39. M.K. Padhy and R.P. Saini, Effect of Size and Concentration of Silt Particles on Erosion of Pelton Turbine Buckets, *Energy*, 2009, **34**(10), p 1477–1483